JTTEE5 23:456–462
DOI: 10.1007/s11666-013-9994-8
1059-9630/$19.00 © ASM International

Cold-Sprayed Al Coating for Corrosion Protection of Sintered NdFeB

Chunchun Ma, Xiaofang Liu, and Chungen Zhou

(Submitted May 20, 2013; in revised form August 27, 2013)

A protective Al coating was achieved on the sintered NdFeB magnet by cold spray. The sprayed Al particles generate plastic deformation and hang together. The thickness of the coating is about 170 μm. The corrosion currents of Al coating and NdFeB without immersion tested by potentiodynamic polarization in 3.5 wt.% NaCl solutions are 1.350×10^{-6} and 4.361×10^{-6} A/cm^2, respectively. X-ray photoelectron spectrometry results confirm that the oxide film is Al_2O_3 and the corrosion process can be derived into two different stages. The Al coating can provide long-term protection for NdFeB effectively.

Keywords cold spray, EIS, metal coatings, passive films, pitting corrosion

1. Introduction

As a new generation of permanent magnetic material with excellent properties, the sintered neodymium-iron-boron (NdFeB) has been widely used in various fields such as electronics, acoustics, automation, communications, and magnetic resonance imaging (Ref 1). However, the presence of the rare earth Nd in the magnet sharply decreases its corrosion resistance, which has seriously hindered and limited its applications in humid conditions (Ref 2, 3). Therefore, it is very significant to improve the corrosion resistance of the NdFeB magnet.

In order to improve the corrosion resistance of the permanent magnets, numerous attempts have been employed, such as the addition of alloying elements (Ref 4, 5) and surface coating (Ref 6-8). Previous works (Ref 9-11) have demonstrated that alloying elements such as Co, Cu, Al, Dy, Nb can improve the corrosion resistance of NdFeB, but deteriorate the magnetic properties of the NdFeB magnet. At present, the surface coating technologies are industrially used by the process of electroplating for its good performance and low processing costs (Ref 2, 12, 13), including Ni, Ni-Cu-Ni, Ni/Al, Ni-Co-TiO_2, etc. However, the electroplating method may lead to some environment problems (Ref 14). Al coating is one of the potential candidates for protection because of its friendly price and good corrosion resistance (Ref 15). In industry, Al coatings deposited by evaporation (Ref 16) and ion vapor deposition (IVD) (Ref 6) have been applied for the protection of NdFeB. However, the Al coatings prepared by evaporation and IVD always present a columnar structure with a high concentration of inter-column defects, which could result in premature failure of the coatings (Ref 17).

As an emerging technique for depositing coatings in the solid state, the cold spray (CS) process has attracted more and more attention. Compared with thermal spray process, the CS only requires less heat input. Therefore, CS is more suitable for spraying materials or substrates which are sensitive to oxidation or heat. In addition, coatings by the method of CS have low porosity and high density, which is very helpful for the corrosion resistance of the coatings (Ref 18-20). However, the corrosion properties of CS Al coating on the sintered NdFeB magnets have not well studied. In this work, sintered NdFeB magnets were coated with Al coating deposited by CS, and the corrosion behavior of the Al coating in NaCl solutions was studied.

2. Experimental Details

Sintered NdFeB specimens (N35, Yingkehongye Co., Ltd, Beijing) with a size of 18 mm × 18 mm × 3 mm were used as substrates in this work. All specimens were in the state of demagnetization. Specimens were ultrasonically cleaned in acetone followed by alcohol to remove the oil stain on the surface. Before cold spraying, the NdFeB magnets were sandblasted first.

Industrial pure aluminum powder (99.5 wt.%) produced by gas atomization was used as feedstock material for coatings. Figure 1 shows the scanning electron microscope (SEM) morphology of the as-purchased Al powders used in the experiment. It can be seen in Fig. 1 that most of the powders present spherical shape and the diameters of the spherical Al powders range from 5 to 60 μm. Deposition of Al coating was carried out in a cold spraying apparatus which could deposit homogeneous coatings onto all surfaces of the specimens with batch treatments. The commercial cold spray system (HCY-1, Russia) was used in these experiments. The spraying distance was maintained at 20-50 mm away from the nozzle exit. As

Chunchun Ma, Xiaofang Liu, and **Chungen Zhou**, School of Materials Science and Engineering, Beijing University of Aeronautics and Astronautics, Beijing 100191, China. Contact e-mail: cgzhou@buaa.edu.cn.

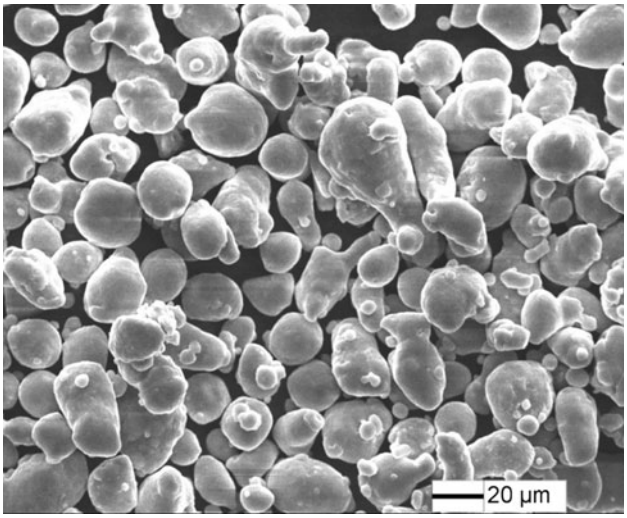

Fig. 1 SEM morphology of the as-purchased Al powders used in the experiment

acceleration and carrier gas for powder feeding, compressed air was pre-heated to 150-250 °C with a stagnation pressure of 1.5-2.5 MPa.

The phase structure of the Al powders and Al coating was analyzed by x-ray powder diffraction (XRD, Model D/Max 2500PC Rigaku, Japan) operated at 40 kV and 40 mA with Cu K_α radiation. And the scan angle was 10-90° with a scan rate of 6°/min. The surface and cross-section morphologies of Al coatings were studied by SEM (CS3400, CamScan, UK). The composition of the surface of Al coating was analyzed by x-ray photoelectron spectrometry (XPS, Axis Ultra, Kratos Analytical Ltd., UK). And the Al coating was ground from 280# to 800# on the sandpapers for the cross-section morphology. The corrosion behavior of Al coatings was determined by potentiodynamic polarization and electrochemical impedance spectroscopy (EIS) tests using a classical three electrodes system. The reference electrode and counter electrode were saturated calomel (SCE) and platinum, respectively. The Al coating or NdFeB specimens were used as working electrode. And all the electrochemical experiments were conducted on the as-sprayed Al coatings surface. The corrosion electrolyte for all the corrosion tests was 3.5 wt.% sodium chloride (NaCl) solutions at room temperature. And the surface area of the specimens exposed for corrosion study was 1 cm^2. The EIS measurements were carried out with signal amplitude of 5 mV, and the frequency range was from 10^5 to 10^{-2} Hz. And the impedance curves were simulated using the software ''ZsimpWin''.

3. Results and Discussion

3.1 Structure and Composition

Figure 2 shows the surface and cross-section morphology of Al coating on sintered NdFeB magnets. Compared

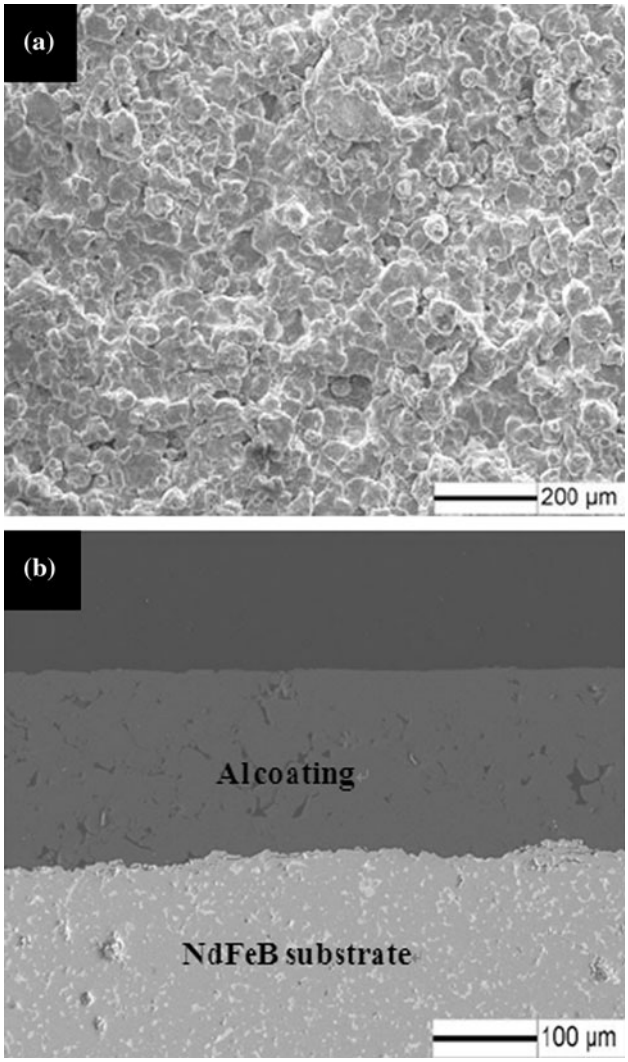

Fig. 2 SEM morphologies of the Al coating (a) surface, (b) cross-section

with Fig. 1, it can be found in Fig. 2(a) that the sprayed Al particles generate plastic deformation and hang together, which could be caused by the high velocity impact during cold spraying. Meanwhile, in Fig. 2(b), it can be seen that the coating is very dense and the thickness is about 170 μm. There are no cracks and other defects found on the interface. And the NdFeB interface becomes irregular, which is from the grit-blasting surface preparation before the CS. Then, the accelerated Al particles impact and embed onto the NdFeB substrate, leading to the plastic deformation on the NdFeB interface and thus inducing excellent bonding.

The XRD patterns of the Al powders and Al coating are shown in Fig. 3. It can be observed that both the Al powders and Al coating exhibit a single Al phase with face-centered cubic (FCC) crystal structure, which indicates that there are no significant oxidations during the cold spraying process.

3.2 Potentiodynamic Curves Measurements

Figure 4 shows the potentiodynamic curves of the NdFeB and the Al coating with different immersion time in 3.5 wt.% NaCl solutions. Corrosion current density (i_{corr}) and corrosion potential (E_{corr}) derived from Fig. 4 are summarized in Table 1. The corrosion current density (i_{corr}) is an important parameter for the evaluation of the corrosion resistance. From Table 1, it can be observed that the i_{corr} of Al coating without immersion (1.350×10^{-6} A/cm^2) is less than 1/3 that of NdFeB (4.361×10^{-6} A/cm^2). It suggests that the Al coating could provide an adequate protection for the NdFeB substrate in 3.5 wt.% NaCl solutions.

As seen in Table 1, the i_{corr} of the Al coating after the immersion for 24 h is higher than that of the Al coating without immersion. The i_{corr} becomes higher which may be attributed to the damage of oxide film formed in the air. With the further immersion, the i_{corr} gradually decreases. This decrease in the sprayed Al coating suggests the interaction of Al and solution to form a new barrier, mainly oxides that prevent solution ion penetration. Therefore, the Al coating can provide long time protection for the NdFeB substrate.

The i_{corr} without immersion of the Al coating by DC magnetron sputtering (Ref 21) is only 0.091 μA/cm^2, which is lower than the i_{corr} of the present Al coating. However, the further study of the Al coating by DC magnetron sputtering (Ref 22) has shown that the Al coating cannot provide long time protection for the NdFeB substrate due to the dissolution of the Nd-rich phase through the open pits and disruption of the matrix phase. Compared to the cold spray Al coatings, the DC coating has a thickness of only about 5 μm, and presents columnar structure with a number of voids distributed at the grain boundaries, which is susceptible to pitting corrosion (Ref 21). Therefore, the Al coating by cold spraying has more potential for protecting the sintered NdFeB.

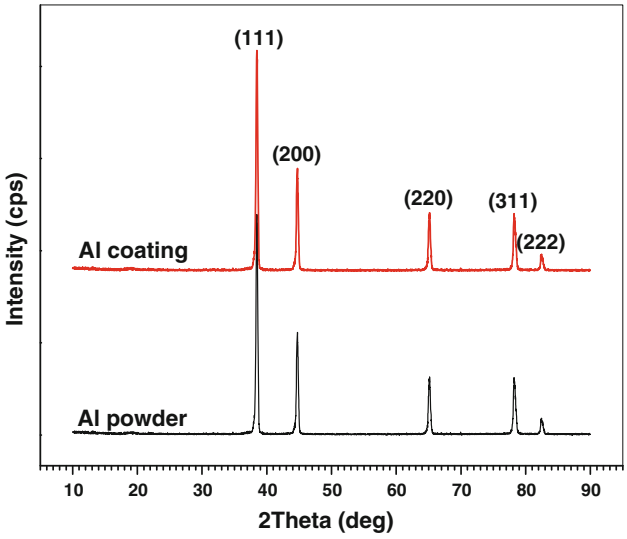

Fig. 3 XRD patterns of the Al powders and cold-sprayed Al coating

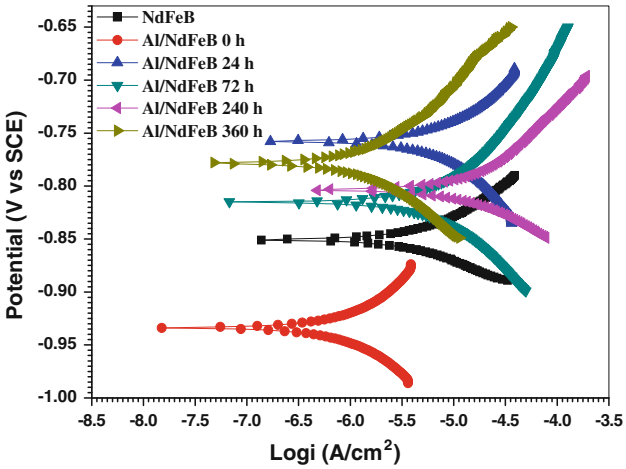

Fig. 4 Potentiodynamic curves of the NdFeB and Al coating with different immersion time in 3.5 wt.% NaCl solutions

3.3 Corrosion Products

Scanning electron microscope surface morphologies of the Al coating after immersing for 24 h and 360 h in 3.5 wt.% NaCl solutions are shown in Fig. 5. As seen in Fig. 5(a), the obvious pits have been found after immersing for 24 h. However, it is clear from Fig. 5(b) that the pits are not observed after an immersion time of 360 h. The elemental composition of the surface of the Al coating was analyzed by XPS. Figure 6 shows the XPS high-resolution spectra of the Al coating after immersing for 0 h, 24 h, and 360 h in 3.5 wt.% NaCl solutions. Figure 6(a) is the Al 2p spectrum and Fig. 6(b) is the O 1s spectrum. In Fig. 6(a), for the Al coating with the immersion time of 0 h and 24 h, the presence of aluminum in the form of Al^{3+} and in metallic state (Al^0) is detected by the Al 2p peaks. However, the metallic state (Al^0) is not found on the surface of the Al coating after immersing for 360 h. The O 1s spectrum shown in Fig. 6(b) are composed of only one peak and the binding energies are 531.49 eV, 532.02 eV, and 532.22 eV for 0 h, 24 h, and 360 h, respectively, which may be due to oxygen in Al-O bonds. By considering the spectra of Al and O, it is proposed that the composition on the Al coating should be Al_2O_3. According to the quantitative analysis of the XPS, the concentration ratio of the Al^{3+} for 0 h, 24 h, and 360 h is 1: 0.86: 1.33. Therefore, the Al coating after immersing

Table 1 Electrochemical parameters calculated from the potentiodynamic curves in Fig. 4

Specimen	Immersion time, h	E_{corr}, V versus SCE	i_{corr}, A/cm^2
NdFeB	0	−0.851	4.361×10^{-6}
Al/NdFeB	0	−0.934	1.350×10^{-6}
Al/NdFeB	24	−0.758	1.134×10^{-5}
Al/NdFeB	72	−0.815	9.88×10^{-6}
Al/NdFeB	240	−0.804	5.321×10^{-6}
Al/NdFeB	360	−0.778	2.178×10^{-6}

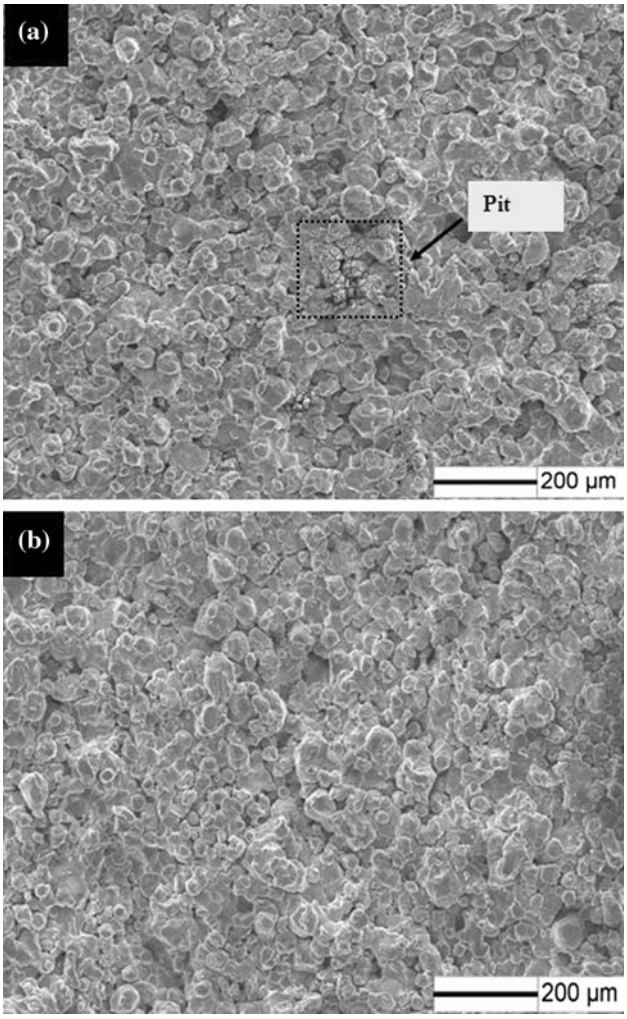

Fig. 5 SEM surface morphologies of the Al coating after immersing in 3.5 wt.% NaCl solutions for 24 h (a) and 360 h (b)

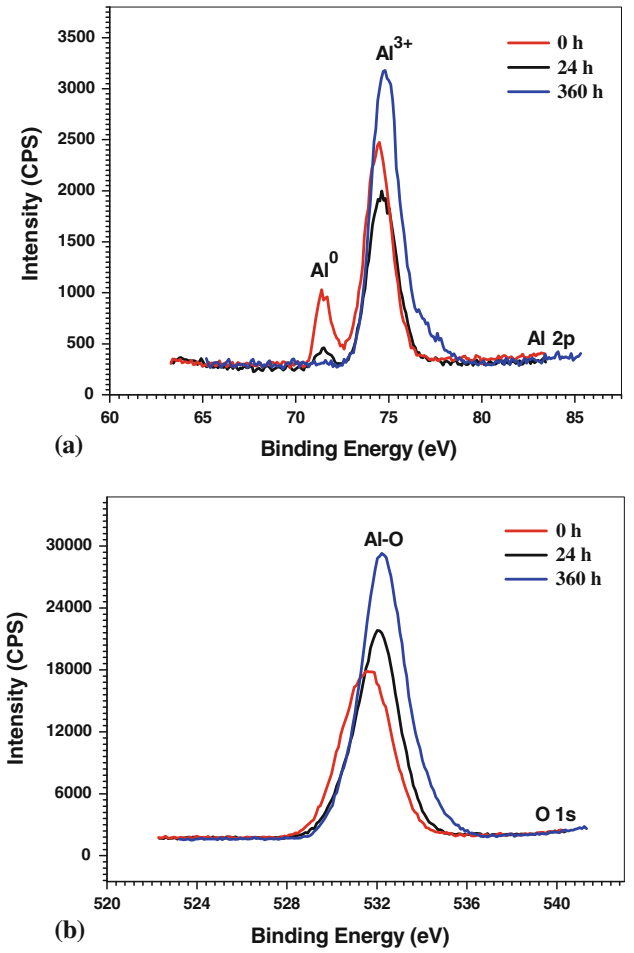

Fig. 6 XPS high-resolution spectra of the Al coating after immersing in 3.5 wt.% NaCl solutions for 0 h, 24 h, and 360 h (a) Al 2p; (b) O 1s

for 24 h, the Al_2O_3 film formed in the air is damaged, and the compact Al_2O_3 film forms again after immersing for 360 h. The formation of the Al_2O_3 film can be expressed by the following equations (Ref 23):

$$Al + H_2O \rightarrow AlOH + H^+ + e \quad \text{(Eq 1)}$$

$$AlOH + H_2O \rightarrow Al(OH)_2 + H^+ + e \quad \text{(Eq 2)}$$

$$Al(OH)_2 \rightarrow AlOOH + H^+ + e \quad \text{(Eq 3)}$$

The total equation is $Al + H_2O \rightarrow AlOOH + 3H^+ + 3e$, in which the AlOOH is $Al_2O_3{\cdot}H_2O$. Though the formation of the oxide film in the present work is different from that of the oxide film ($Al(OH)_3$) on the Al coating by DC magnetron sputtering and the IBAD-Al-coating in the previous study (Ref 24), the Al_2O_3 and $Al(OH)_3$ act as the barrier that delays the penetration of the corrosion electrolyte. Therefore, the corrosion process of Al coating immersed in 3.5 wt.% NaCl solutions can be divided into two stages. In the first stage (0-24 h) Al_2O_3 film formed in the air is damaged, and in the second stage (24-360 h) the compact Al_2O_3 film forms again.

3.4 Electrochemical Impedance Spectroscopy Measurements

The evolution of the Nyquist diagrams for NdFeB substrate and Al coating with different immersion time in 3.5 wt.% NaCl solutions are presented in Fig. 7. As illustrated in Fig. 7, the NdFeB consists of one high frequency capacitance loop and one low frequency inductance loop, while the Al coating includes only one high frequency capacitance loop without immersion. The inductance loop of the substrate implies that pitting corrosion is formed on NdFeB surface. Meanwhile, the diameter of the high frequency capacitance loop of the Al coating without immersion is much larger than that of the substrate (in Fig. 7). It suggests that the Al coating could provide adequate protection for NdFeB substrate, which is in accordance with the potentiodynamic curves measurements.

In Fig. 7, it can also be found that the semicircle diameter dramatically decreases with immersion time from 0 to 24 h, and with the extension of the immersion time, the semicircle diameter gradually increases. Therefore, the EIS diagrams show the different characteristics in the two stages identified from the above SEM and XPS results. In order to discuss the corrosion mechanisms clearly, the equivalent circuits are presented in Fig. 8. The models are obtained after fitting the data from Nyquist diagrams using the ZsimpWin software (Ref 25, 26). The constant phase angle element (CPE, designated as Q) is used instead of the pure capacitance, and its admittance (Y_Q) can be expressed as (Ref 27):

$$Y_Q = Y_0(j\omega)^n, \quad \text{(Eq 4)}$$

where j is the imaginary number and ω is the angular frequency. Y_0 is the admittance constant and n is the empirical exponent of the CPE, respectively. Warburg impedance (designated as W) is used to model semi-infinite diffusion. The admittance of Warburg impedance (Y_W) can be expressed as:

$$Y_W = Y_0(j\omega)^{1/2}, \quad \text{(Eq 5)}$$

where Y_0 is the admittance constant of the Warburg impedance.

As in previous studies of equivalent circuit for oxide films on metals (Ref 28-30), the model R(Q(R(QR))) (Fig. 8a) is employed to simulate the Nyquist plots in the first stage (0-24 h). In the equivalent circuit shown in Fig. 8(a), R_s represents the solution resistance; Q_1 represents the oxide film capacitance; R_c is the electrical resistance to the ionic current through the defects in the Al oxide film; Q_2 is the double-layer capacitance of electrochemical reaction and R_{ct} is the charge transfer resistance. The fitted results are listed in Table 2. It can be seen from Table 2 that the simulated values of both R_c and R_{ct} decrease due to the effects of the pitting corrosion.

In the second stage, the Nyquist diagrams shown in Fig. 7 have diffusion-controlled characteristics at low frequencies connecting to a capacitive semicircle at high frequencies. The model R(Q(W(QR))) (Fig. 8b) is employed to simulate the Nyquist diagrams of the Al coating after immersing for 72 h, 240 h, and 360 h. In the equivalent circuit shown in Fig. 8(b), R_s represents the solution resistance; Q_3 represents the oxide film capacitance; Q_4 is the double-layer capacitance of electrochemical reaction; R_{ct} is the charge transfer resistance; Warburg impedance W is employed to simulate the diffusion-controlled process at low frequencies. The simulated values are presented in Table 3. The values of R_{ct} in the second stage (72, 240, and 360 h) gradually increase and are larger than that of the R_{ct} of Al coating immersing for 24 h, which suggests that after immersing for 72 h a stable barrier gradually forms on the surface of the Al coating and then prevents the solution ion penetration effectively. This result agrees with the potentiodynamic polarization curves and the XPS results. Therefore, the Al coating on the NdFeB could provide excellent corrosion resistance. And the excellent corrosion resistance is attributed to the formation of Al_2O_3 oxide film.

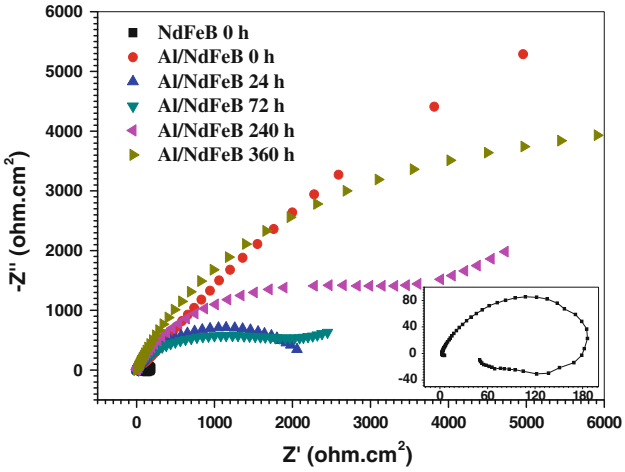

Fig. 7 Nyquist plots of the NdFeB and Al coating with different immersion time in 3.5 wt.% NaCl solutions

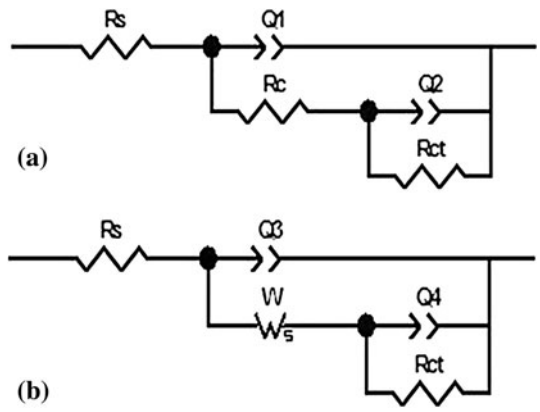

Fig. 8 Equivalent circuits for EIS data in (a) the first stage and (b) the second stage, respectively

Table 2 Electrochemical parameters obtained from equivalent circuit in Fig. 8(a) by simulation

			Q_1			Q_2		
Specimen	**Immersion time, h**	**R_s, ohm cm²**	**Y_0-Q_1, μS/cm² sⁿ**	***n***	**R_c, ohm cm²**	**Y_0-Q_2, μS/cm² sⁿ**	***n***	**R_{ct}, ohm cm²**
Al/NdFeB	0	9.513	63.97	0.985	138.1	621.7	0.6444	30650
Al/NdFeB	24	4.397	17.22	0.992	91.98	141.7	0.6424	2249

Table 3 Electrochemical parameters obtained from equivalent circuit in Fig. 8(b) by simulation

Specimen	Immersion time, h	R_s, ohm cm^2	Q_3		Y_0-W, μS/cm^2 s^n	Q_4		R_{ct}, ohm cm^2
			Y_0-Q_3, μS/cm^2 s^n	n		Y_0-Q_4, μS/cm^2 s^n	n	
Al/NdFeB	72	4.436	25.33	0.896	6068	239.1	0.4483	2278
Al/NdFeB	240	4.469	20.64	0.928	1498	167.3	0.6992	3152
Al/NdFeB	360	4.274	24.75	0.964	494.7	158.3	0.7787	5389

4. Conclusions

The cold-sprayed Al coating was successfully achieved on NdFeB substrates. In the process of spraying, the Al particles generated plastic deformation and deposited on the surface of NdFeB. The coating was very dense and its thickness was 170 μm. According to the measurements of potentiodynamic curves and electrochemical impedance spectroscope in 3.5 wt.% NaCl solution, the cold-sprayed Al coating could improve the corrosion resistance of the sintered NdFeB magnets and provide long time protection to the NdFeB substrates due to the formation of Al_2O_3 film. Therefore, Al coating deposited by cold spraying seemed as a feasible method for protecting the sintered NdFeB magnets.

Acknowledgments

This work was supported by a grant from the National High Technology Research and Development Program of China under the contract of 2012BAE02B01.

References

1. M. Sagawa, S. Fujimura, N. Togawa, H. Yamamoto, and Y. Matsuura, New Material for Permanent Magnets on a Base of Nd and Fe, *J. Appl. Phys.*, 1984, **55**, p 2083-2087
2. Y.W. Song, H. Zhang, H.X. Yang, and Z.L. Song, A Comparative Study on the Corrosion Behavior of NdFeB Magnets in Different Electrolyte Solutions, *Mater. Corros.*, 2008, **59**, p 794-801
3. M. Rada, A. Gebert, I. Mazilu, K. Khlopkov, O. Gutfleisch, L. Schultz, and W. Rodewald, Corrosion Studies on Highly Textured Nd-Fe-B Sintered Magnets, *J. Alloys Compd.*, 2006, **415**, p 111-120
4. H. Bala, G. Pawlowska, S. Azymura, V.V. Sergeev, and Y.M. Rabinovich, Corrosion Characteristics of NdFeB Sintered Magnets Containing Various Alloying Elements, *J. Magn. Magn. Mater.*, 1990, **87**, p L225-L259
5. S. Sunada, K. Majima, Y. Akasofu, and Y. Kaneko, Corrosion Assessment of Nd-Fe-B Alloy with Co Addition Through Impedance Measurements, *J. Alloy Compd.*, 2006, **408-412**, p 1373-1376
6. P. Mitchell, Corrosion Protection of NdFeB Magnets, *IEEE Trans. Magn.*, 1990, **26**, p 1933-1935
7. Z. Chen, A. Ng, J.Z. Yi, and X.F. Chen, Multi-Layered Electroless Ni-P Coatings on Powder-Sintered Nd-Fe-B Permanent Magnet, *J. Magn. Magn. Mater.*, 2006, **302**, p 216-222
8. T. Minowa, M. Yoshikawa, and M. Honshima, Improvement of the Corrosion Resistance on Nd-Fe-B Magnet with Nickel Plating, *IEEE Trans. Magn.*, 1989, **25**, p 3776-3778
9. A.S. Kim and F.E. Camp, A High Performance Nd-Fe-B Magnet with Improved Corrosion Resistance, *IEEE Trans. Magn.*, 1992, **28**, p 2151-2153
10. W. Fernenge, W. Rodewald, R. Blank, P. Schrey, M. Katter, and B. Wall, The Influence of Co on the Corrosion Resistance of Sintered Nd-Fe-B Magnets, *J. Magn. Magn. Mater.*, 1999, **196**, p 288-290
11. L.Q. Yu, Y.H. Wen, and M. Yan, Effects of Dy and Nb on the Magnetic Properties and Corrosion Resistance of Sintered NdFeB, *J. Magn. Magn. Mater.*, 2004, **283**, p 353-356
12. X.K. Yang, Q. Li, S.Y. Zhang, X.K. Zhong, Y. Dai, and F. Guo, Electrochemical Corrosion Behaviors and Protective Properties of Ni-Co-TiO_2 Composite Coating Prepared on Sintered NdFeB Magnet, *Mater. Corros.*, 2010, **61**, p 618-625
13. H.Z. Rao, G.H. Li, and P.L. Wang, Protective Coating for NdFeB Permanent Magnet Materials, *Chin. Rare Earths*, 1999, **20**, p 40-43
14. K.O. Legg, M. Graham, P. Chang, F. Rastagar, A. Gonzales, and B. Sartwell, The Replacement of Electroplating, *Surf. Coat. Technol.*, 1996, **81**, p 99-105
15. J.K. Chang, S.Y. Chen, W.T. Tsai, M.J. Deng, and I.W. Sun, Electrodeposition of Aluminum on Magnesium Alloy in Aluminum Chloride ($AlCl_3$)-1-ethyl-3-methylimidazolium Chloride (EMIC) Ionic Liquid and Its Corrosion Behavior, *Electrochem. Commun.*, 2007, **9**, p 1602-1606
16. N.C. Ku, C.D. Qin, C.C. Yu, and D.H.L. Ng, Corrosion Resistance of NdFeB Magnets Coated by Al, *IEEE Trans. Magn.*, 1996, **32**, p 4407-4409
17. D.P. Monaghan, D.G. Teer, P.A. Logan, K.C. Laing, R.I. Bates, and R.D. Arnell, An Improved Method for the Deposition of Corrosion-resistant Aluminium Coatings for Aerospace Applications, *Surf. Coat. Technol.* 1993, **60**, p 592-596
18. A.P. Alkhimov, V.F. Kosarev, and A.N. Papyrin, Gas-Dynamic Spraying: An Experimental Study of the Spraying Process, *J. Appl. Mech. Tech. Phys.*, 1998, **39**, p 318-323
19. V.K. Champagne, D.J. Helfritch, and P.F. Leyman, Magnesium Repair by Cold Spray, *Plat. Surf. Finish.*, 2008, **95**, p 19-28
20. Y.S. Tao, T.Y. Xiong, C. Sun, H. Jin, H. Du, and T.F. Li, Effect of α-Al_2O_3 on the Properties of Cold Sprayed Al/α-Al_2O_3 Composite Coatings on AZ91D Magnesium Alloy, *Appl. Surf. Sci.*, 2009, **256**, p 261-266
21. S.Z. Mao, H.X. Yang, J.L. Li, H.G. Ying, and Z.L. Song, The Properties of Aluminium Coating on Sintered NdFeB by DC Magnetron Sputtering, *Vacuum*, 2011, **85**, p 772-775
22. S.D. Mao, H.X. Yang, Z.L. Song, J.L. Li, H.G. Ying, and K.F. Sun, Corrosion Behavior of Sintered NdFeB Deposited with an Aluminium Coating, *Corros. Sci.*, 2011, **53**, p 1887-1894
23. S.Z. Song and Z.L. Tang, An Electrochemical Impedance Analysis on Aluminum in 3.5% NaCl Solution, *J. Chin. Soc. Corros. Prot.*, 1996, **16**, p 127-132
24. S.D. Mao, H.X. Yang, J.L. Li, F. Huang, and Z.L. Song, Corrosion Properties of Aluminium Coatings Deposited on Sintered NdFeB by Ion-Beam-Assisted Deposition, *Appl. Surf. Sci.*, 2011, **57**, p 5581-5585
25. M. Yue, J.X. Zhang, W.Q. Liu, and G.P. Wang, Corrosion Kinetics of Spark Plasma Sintering Nd-Fe-B Magnets in Different Electrolytes, *IEEE Tran. Magn.*, 2005, **41**, p 3892-3894
26. Y.S. Huang, X.T. Zeng, X.F. Hu, and F.M. Liu, Corrosion Resistance Properties of Electroless Nickel Composite Coatings, *Electrochim. Acta*, 2004, **49**, p 4313-4319
27. E. Barsoulkov, and J.R. Macdonald, *Impedance Spectroscopy Theory, Experiment, and Application*, 2nd ed., Wiley, Hoboken, NJ, 2005
28. J.B. Bessone, D.R. Salinas, C.E. Mayer, M. Ebert, and W.J. Lorenz, An EIS Study of Aluminium Barrier-Type Oxide Films Formed in Different Media, *Electrochim. Acta*, 1992, **37**, p 2283-2290

29. J.F. Zhang, W. Zhang, C.W. Yan, K.Q. Du, and F.H. Wang, Corrosion Behaviors of Zn-Al-Mn Alloy Composite Coatings Deposited on Magnesium Alloy AZ31B (Mg-Al-Zn), *Electrochim. Acta*, 2009, **55**, p 560-571

30. H. Zhang, Y.L. Zhao, and Z.D. Jiang, Effects of Temperature on the Corrosion Behavior of 13Cr Martensitic Stainless Steel During Exposure to CO_2 and Cl^- Environment, *Mater. Lett.*, 2005, **59**, p 3370-3374